Astron. Astrophys. 324, 725–734 (1997)

ASTRONOMY AND ASTROPHYSICS

A kinetic model of the solar wind with Kappa distribution functions in the corona

M. Maksimovic[1], **V. Pierrard**[2], **and J.F. Lemaire**[2]

[1] Département de Recherche Spatiale et Unité de Recherche associée au CNRS 264, Observatoire de Paris, Section de Meudon, F-92195 Meudon Principal Cedex, France (internet:maksimovic@obspm.fr)
[2] Institut d'Aéronomie Spatiale,3 Ave. Circulaire, B-1180, Bruxelles, Belgique

Received 3 June 1996 / Accepted 23 December 1997

Abstract. A kinetic model of the solar wind based on Kappa velocity distribution functions for the electrons and protons escaping out of the corona is presented. The high velocity particles forming the tail of these distribution functions have an enhanced phase space density compared to a Maxwellian. The existence of such velocity distribution functions have been introduced in the pioneering work of Scudder (1992a,b) to explain the high temperature of the coronal plasma. The first results obtained with this new kinetic model of the solar wind are very encouraging, indeed they fit better many major features observed in the solar wind than earlier models: e.g. the large bulk velocities observed in high speed streams emitted out of coronal regions where the plasma temperature is smaller, and the low speed solar wind originating in the hotter equatorial regions of the solar corona. This new kinetic model is also able to predict the high speed solar wind streams without unreasonably large coronal temperatures and without additional heating of the outer region of the corona, as it is needed in hydrodynamic models to achieve the same solar wind speed.

Key words: solar wind – Sun: corona – acceleration of particles – plasmas

1. Introduction

The velocity distribution functions of the solar wind electrons and protons have to be solutions of the Boltzmann equation, or more precisely of the Fokker-Planck equation in the case when binary collisions are less important than multiple small angle scattering. Based on this statement, two approaches may be used to model the solar wind global thermodynamics, each of them being built on equations derived from the Boltzmann or the Fokker-Planck equations. These approaches correspond to two extreme regimes of the Knudsen number K_n, which is defined as the ratio of the particle mean free path and the density scale height. The first one is the classical hydrodynamic approach. It is based on the Euler or Navier-Stokes approximations, which are applicable under the assumption that K_n is much smaller than unity, i.e., that the medium is collision-dominated. The second one is the exospheric (collisionless) approach, which is based on the Vlasov equation; it is then assumed that $K_n \rightarrow \infty$, i.e., that the medium is collisionless.

It is well known that the solar wind is neither a collision-dominated medium nor a collisionless one. Indeed, in the solar wind at the earth orbit, the values of the electron and the proton Knudsen numbers are roughly equal to unity (Montgomery et al. 1968; Hundhausen 1972). This means that, strictly speaking, neither the hydrodynamic approach and nor the exospheric or pure collisionless one are truely appropriate to model the global expansion and thermodynamics of the solar wind. Nevertheless, each of these two extreme approaches yielded models whose results can explain some, although not all, of the main observational features of the solar wind.

1.1. The hydrodynamic approach

Historically, the hydrodynamic approach of the solar wind has been introduced by Parker (1958). He described the steady state expansion of a thermally driven electron-proton plasma flow out of the hot solar corona. Following Parker's initial idea, many other authors have proposed more elaborated hydrodynamic or magnetohydrodynamic descriptions for the last fourty years. The aims of these works were to take into account the effects of thermal conductivity and viscosity, or the particular topology of the interplanetary magnetic field, to describe better the general solar wind observations at the earth's orbit. Two-fluids models have also been used to take into account the different electron and ion temperatures and bulk velocities observed at 1 AU in the solar wind (Sturrock & Hartle 1966; Whang et al. 1966; Hartle & Sturrock 1968; Cuperman & Harten 1970, 1971; Hartle & Barnes 1970; Wolff et al. 1971).

One of the major shortcomings common to all these hydrodynamic models is that they never predict solar wind velocities of 600-800 km/s at 1 AU, without invoking ad-hoc deposition

Send offprint requests to: M. Maksimovic

of momentum and/or additional dissipation of energy in the corona; in general this additional energy is assumed to be carried out of the photosphere into the corona by MHD waves (see Leer et al. 1982 for a review).

1.2. The exospheric approach

Among the kinetic approaches, the purely collisionless one is generally called the exospheric approach. Two classes of exospheric solar wind models have been developed during the last fourty years. The first one is the solar breeze model. It was proposed by Chamberlain (1960) who suggested that the protons with a velocity exceeding the critical escape velocity evaporate like neutral particles escape out of a planetary atmosphere (Jeans 1923, Brandt & Chamberlain 1960). Thus Chamberlain suggested that the radial expansion of the solar corona results from the thermal evaporation of the hot coronal protons out of the gravitational field of the Sun. Following Chamberlain's work, many authors have investigated the kinetic evaporation of the corona (see Lemaire & Scherer,1973 for a review). They all assumed that the interplanetary electric field is equal to the so-called Pannekoek-Rosseland field (Pannekoek 1922; Rosseland 1924), which is appropriate for an ionosphere or ion-exosphere in hydrostatic equilibrium, when the electrons and protons have the same temperature distributions and no upward or downward bulk motions. Using the Pannekoek-Rosseland electrostatic potential in these early exospheric models for the coronal evaporation yields, as in Chamberlain's solar breeze model, too small solar wind expansion speeds as compared to the observations. On the contrary, Parker's hydrodynamic model of the coronal expansion provided theoretical results supporting the existence of the observed supersonic wind speeds of 300 - 500 km/s at 1 AU. This point marked the begining of the growing supremacy of the hydrodynamic approach and the demise of the kinetic one, for a period of almost 30 years.

However, an important step for the exospheric approach of the solar wind have been achieved by Lemaire & Scherer (1969, 1971b) and Jockers (1970) who demonstrated that, for an expanding atmosphere (i.e., not in hydrostatic equilibrium), the magnitude of the interplanetary electric potential is substantially greater than the Pannekoek-Rosseland value. Using this more realistic potential, Lemaire & Scherer (1971b) developed a new kinetic model for the solar ion-exosphere and obtained supersonic expansion velocities for the solar wind at 1 AU. Their collisionless kinetic model predicted also correctly the quiet solar wind density, bulk velocity and average temperatures observed at 1 AU, as well as correlations between these physical quantities and better than hydrodynamic models available at that epoch (see Table 2 in Lemaire & Scherer 1971b). Only one major disagreement was pointed out in their paper. This was the ratio of the parallel and perpendicular pressures or temperatures of the electrons and protons predicted in their exospheric model, which was much too large compared to those observed. But, following the work of Griffel & Davis (1969), Lemaire & Scherer (1971b) concluded that this limitation of their zero order kinetic model was an inherent consequence of neglecting the cumulative effect of small pitch angle deflections due to Coulomb collisions which necessarily tends to reduce the anisotropy of the particle velocity distributions.

First order kinetic effects have been proposed by Hollweg (1976) using saturated fluxes instead of the classical Spitzer-Härm expressions for the heat conductivity coefficient. An even better description of the heat flow has been proposed by Olbert (1982). Both kinetic heat flux expressions were then used in various versions of the hydrodynamic energy transport equations, but not in any full fledged first order kinetic approach based on the collisional Fokker-Planck equation.

Recently, Scudder (1992a,b) proposed a new mechanism to explain the high temperature observed in the corona. This mechanism, called "the velocity filtration effect", works under the assumption that the velocity distribution function (VDF) of the ions and the electrons in the chromosphere, and therefore in the corona, is a non-Maxwellian, e.g. a generalized Lorentzian or Kappa function. Following Scudder's work, Pierrard & Lemaire (1996) developed a generalized Lorentzian ion-exosphere model, which accounts the observed ion and electron positive temperature gradients between the topside ionosphere and the plasmasphere. Scudder's, and Pierrard & Lemaire's works may confer new momentum to the long dismissed kinetic approaches of the solar wind: this is what we plan to show in the present paper. In Sect. 2, we give the basics of the exospheric formulation used, which is built on the Lemaire & Scherer (1970; 1971a) and Pierrard & Lemaire (1996) kinetic models of an ion-exosphere. We describe below the implementation of this model for the solar wind under the assumption of Kappa velocity distribution functions in the corona. In Sect. 3, we present our results, with emphasis on the fact that high speed solar wind streams may be explained by the present model without the need of an additional heating energy source for the corona, a conclusion which is supporting one of Scudder's early contention. Finally, a summary is presented in Sect. 4.

2. The basics of the model

As indicated above, the present work is based on the kinetic/exospheric model of the ion-exosphere originally developed by Lemaire & Scherer (1970; 1971a) for geomagnetic field lines open to the magnetospheric tail. This model, initially dedicated to the study of the polar wind, had subsequently been applied to model the solar wind (Lemaire & Scherer 1971b), with the assumption of Maxwellian VDF's for the protons and electrons at the top of the collision-dominated part of the corona. In the present work, we depart from these earlier models by using new exospheric models based on generalized Lorentzian or Kappa VDF for the protons and for the electrons at an exobase altitude, as in the polar wind model recently proposed by Pierrard & Lemaire (1996).

2.1. The exobase location

In zero order kinetic approximations, or exospheric models, two separate regions are considered: first, the collision-dominated

barosphere at low altitude, in which the particles are assumed to be in hydrostatic/hydrodynamic equilibrium, and secondly, an exosphere in which the collision rate between particles is assumed to be negligibly small. These two extreme Knudsen number regimes are separated by a surface which is called the exobase. The exobase location will be determined, as initially proposed by Jeans (1923) for neutral particles and by Spitzer (1949) for charged particles, by the altitude where the Knudsen number is equal to unity. So in the present solar wind model, the exobase distance from the Sun r_0 is defined as the distance where the Coulomb mean free path (m.f.p.) becomes equal to the local density scale height H defined by:

$$H = \left(-\frac{d \ln n}{dr} \right)^{-1} \tag{2.1}$$

where n is the electron density as determined from eclipse observations.

For the coronal temperatures and densities considered in this paper, the classical Spitzer's (1962) proton deflection m.f.p. is given by:

$$\lambda_p \approx 7.2\ 10^7\ \frac{T_p^2}{n} \tag{2.2}$$

where λ_p is given in meters, the proton temperature T_p in Kelvins and the density n in m^{-3}. We consider the corona and the solar wind plasma composed only of protons and electrons, so that we have $n_e = n_p = n$ as implied by quasi-neutrality.

From the measurements of the intensity and polarization of the electron-scattered white light coronal radiation, it is possible to determine the radial distribution of the electron density in the corona. In Fig. 1, three examples of such radial density profiles by Pottasch (1960), Newkirk (1967) and Withbroe (1988) are given. The differences between these three density profiles, corresponding all to quiet coronal regions, are relatively small. In order to obtain the radial distribution of the density scale height H in the corona, we have first determined by interpolation an average radial density profile from the three sets of observed densities. The result is given by the solid line in Fig. 1.

Hence, for a given value of the proton temperature $T_p(r_{p0})$, the radial distance (r_{p0}) of the proton exobase where $\lambda_p = H$ can be determined by solving iterativelly the equation

$$7.2\ 10^7\ T_p^2(r_{p0}) = n^2(r_{p0}) \left(-\frac{dn(r)}{dr} \right)^{-1}_{r=r_{p0}} \tag{2.3}$$

for the interpolated electron density profile $n(r)$

The exobase altitude for the electrons with a speed equal to the mean thermal velocity $(8kT_e/m_e\pi)^{1/2}$, can be determined by using the Coulomb deflection m.f.p. λ_e of thermal electrons in a hydrogen plasma which is defined by:

$$\lambda_e = 0.416(T_e/T_p)^2 \lambda_p \tag{2.4}$$

For equal electron and proton temperatures, λ_e is smaller than λ_p so that the electron exobase r_{e0} is located at slightly higher distances than r_{p0}. For convenience, we will assume here that the escaping electrons and protons come from the same exobase $r_0 = r_{p0} = r_{e0}$, and therefore that electron and proton Coulomb deflection m.f.p. are equal at r_0. This implies from (2.4) that, at the exobase, the electron and proton temperatures are related by $T_{e0} = \gamma \times T_{p0}$, where $\gamma = 1.55$. This latter condition can be relaxed in future applications of our model, but is not unreasonable in view of the electron and ion temperatures deduced from various coronal observations. If $\gamma > 1.55$, the electron m.f.p. would be larger than the proton m.f.p., and the electron exobase at a higher altitude than the proton exobase.

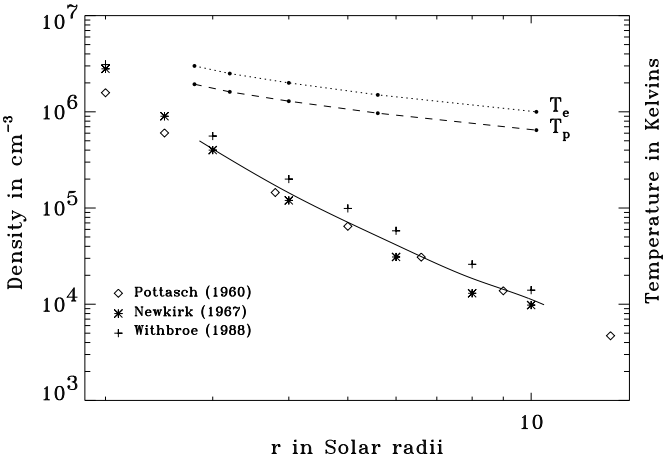

Fig. 1. Different radial density profiles in the corona as given by Pottasch (1960) (diamonds), Newkirk (1967) (stars) and Withbroe (1988)(crosses) and the average radial density profile (solid line) determined by interpolation from these three sets. The electron (dotted line) and proton (dashed line) radial temperature profiles are determined by equaling the density scale height and the particle mean free paths (see in the text). The points on the temperatures curves correspond to the set of exobase conditions given in Table 1.

In order to explore the effect of various coronal conditions, we have defined five different sets of exobase conditions. First we start with a given initial electron exobase temperature T_{e0}. Then T_{p0} is determined by $T_{e0}/1.55$, n_0 and r_0 are obtained by solving (2.3), using the density profile of Fig. 1. The five sets of exobase conditions are given in Table 1. T_{e0} has been chosen in the temperature range from 1 to 3×10^6 K. We have also calculated the classical Coulomb electron collision time (Spitzer, 1962) $t_{ce} = 1.7\ 10^4\ T_e^{3/2}/n$ for the different exobase altitudes. The values of these characteristic collision times for momentum transfert between electrons in a plasma are also reported in Table 1, togheter with the values of the particle m.f.p. $\lambda = H$. Note also that if we use in (2.3) a typical density profile for coronal hole regions (Withbroe 1988) instead of that given in Fig. 1, the exobase altitudes are lower than in Table 1 but the general results of the model presented in the following remain roughtly the same.

Table 1. The five sets of exobases boundary conditions

	T_{e0} ($\times 10^6$ K)	T_{p0} ($\times 10^6$ K)	n_0 ($\times 10^{10}$ m^{-3})	r_0 ($\times r_\odot$)	$t_{ce} \propto T_{e0}^{3/2}/n_{e0}$ ($\times$ sec.)	$\lambda = H$ ($\times r_\odot$)
A	1.0	0.6	1.1	10.2	1520	3.4
B	1.5	1.0	5.2	5.6	590	2.0
C	2.0	1.3	14.7	4.0	320	1.2
D	2.5	1.6	31.4	3.2	210	0.8
E	3.0	1.9	55.4	2.8	160	0.7

2.2. The kinetic model description

In the exospheric models of the solar wind, the particles emitted at the exobase with a given velocity v_0 move freely in the exosphere under the influence of the solar gravitational field $\Phi_g(r) = -GM_\odot/r$, an interplanetary electric potential $\Phi_E(r)$ and the interplanetary magnetic field $B(r)$; r being the radial heliocentric distance and $M_\odot$ the solar mass.

If the collisions are neglected in the exosphere, the Boltzmann or Fokker-Planck equations are reduced to Vlasov equation. As a consequence of Liouville's theorem, any function $f(\mathscr{E}, \mu, ...)$, of the constants of the motion ($\mathscr{E}$, μ,...) of particles, is a solution of the Vlasov equation. In the absence of collisions, the total energy $\mathscr{E}$ of the particles is conserved:

$$\mathscr{E} = \frac{1}{2}mv^2 + m\phi_g(r) + Ze\phi_E(r) = \frac{1}{2}mv_0^2 + m\phi_g(r_0) + Ze\phi_E(r_0) \quad (2.5)$$

where v is the velocity of a particle at a location r in the exosphere, v_0 its velocity at the exobase r_0 and Ze its electric charge. In the presence of a magnetic field, the charged particles spiral along magnetic field lines. When their gyroradius is small compared to the length characterizing the inhomogeneities of the magnetic field distribution, the magnetic moment of the particles,

$$\mu = \frac{mv_\perp^2}{2B(r)} = \frac{mv_{\perp 0}^2}{2B(r_0)}, \quad (2.6)$$

where $v_\perp$ and $v_{\perp 0}$ are the components of the velocities $\mathbf{v}$ and $\mathbf{v_0}$ perpendicular to $\mathbf{B}$, is an adiabatic invariant. Altough μ is not a true constant of the motion, one can assume that it is conserved to a good approximation for all electrons and ions in the solar wind, since their gyroradius is small compared to the magnetic field scale height. Note that for neutral particles the angular momentum is conserved and is in this case the second constant of motion (Brandt & Chamberlain 1960).

The trajectories of the particles moving along magnetic field lines depend on their velocity and pitch angle at the exobase. According to the Lemaire & Scherer's (1970; 1971a) terminology, four different classes of trajectories can be identified: trapped, incoming, escaping and ballistic particles (see Tables I and II in Lemaire & Scherer 1971a). In the present application to the solar wind, we consider only electrons on escaping, ballistic and trapped trajectories, and protons on escaping trajectories. Indeed, due to the postulated absence of collisions above the exobase, no particles, in principle, are backscattered in the downward loss cone.

Once a VDF f_0 is assumed at the exobase level r_0, the VDF f at any location r in the exosphere is uniquely determined by Liouville's theorem. The VDFs $f_e(\phi_E(r))$ and $f_p(\phi_E(r))$ are functions of the electric potential at r, $\phi_E(r)$, as well as all the moments of these VDFs, and in particular the electron and proton densities $n_e(\phi_E)$ and $n_p(\phi_E)$. The quasi-neutrality condition $n_e(\phi_E) = n_p(\phi_E)$ is then used to determine, by an iterative method, the value of ϕ_E at any altitude r in the exosphere. The iterative process is stopped when the estimation of $\phi_E(r)$ is adequate to a required precision. Then, it is possible to determine the values of all the other moments of the VDFs, i.e., the flux of particles, their pressure, or their temperatures at any distance r, by integrations of the VDF over the velocity space for both the electrons and the ions. On the contrary, if $n_e(\phi_E) \neq n_p(\phi_E)$, to the required precision, then a new iteration is needed to calculate $\phi_E(r)$.

Strictly speaking, one should solve Poisson's equation instead of imposing quasi-neutrality in the previous iteration process. But for scales much greater than the Debye length, which is the case here, the quasi-neutrality condition provides a very good first approximation for the electrostatic potential distribution in the solar wind (see Lemaire et al. 1991).

Finally, we have neglected Sun's rotation in the present work, by assuming a radial interplanetary magnetic field $B(r)$ varying as r^{-2}. This assumption can be relaxed but at the expenses of tedious mathematical development. Based on earlier attemps by Chen et al. (1972), we have considered that such an effort is not essential in the framework of this first paper on this topic. It is probably not worth the effort, firstly, because $B(r)$ is roughly radial up to 1 AU, and secondly, because,as shown by Chen et al. (1972), the introduction of a spiral magnetic field distribution $B(r)$ modifies only the temperature anisotropies (by diminishing them) but not the other parameters, as the density, bulk velocity and the average temperature.

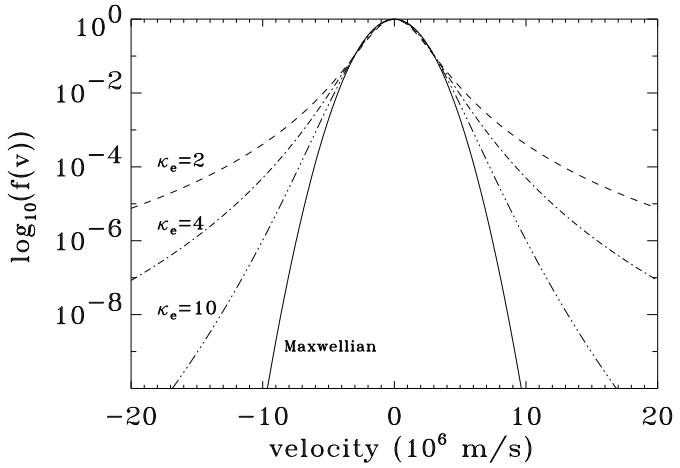

Fig. 2. Different examples of Kappa functions, all normalized to the same value at $v = 0$: $f(0) = 1$. One can see that in the limit $\kappa \to +\infty$, the functions degenerates to a Maxwellian or Gaussian function (solid line).

2.3. Why using a Kappa distribution ?

The Maxwellian VDF is not the only solution of the Vlasov equation: there are an infinite number of collisionless solutions. The generalized Lorentzian or Kappa function f_κ is one of them. It is defined by:

$$f^\kappa(v) = \frac{n}{2\pi(\kappa v_\kappa^2)^{3/2}} \frac{\Gamma(\kappa+1)}{\Gamma(\kappa-1/2)\Gamma(3/2)} \left(1 + \frac{v^2}{\kappa v_\kappa^2}\right)^{-(\kappa+1)} \quad (2.7)$$

where $\Gamma(x)$ is the Gamma function and v_κ is an equivalent thermal speed, related to the equivalent temperature $T_\kappa = m\langle v^2\rangle/3k$ by:

$$v_\kappa = \left(\frac{(2\kappa-3)}{\kappa}\frac{kT_\kappa}{m}\right)^{1/2} \quad (2.8)$$

Fig. 2 illustrates different examples of Kappa functions. They are all normalized to the same value at $v = 0$: $f(0) = 1$. For velocities v smaller or comparable to v_κ, the Kappa VDF, for any value of $\kappa \geq 2$, is rather close to a Maxwellian having the same thermal speed. However, the equivalent Kappa temperature T_κ is related to the Maxwellian one T_M, by $T_\kappa = \frac{\kappa}{\kappa-3/2}T_M$. For $v \gg v_\kappa$, the Kappa VDF decreases with v as a power law ($f^\kappa \propto v^{-\kappa}$). From Fig. 2 we can also see that in the limit $\kappa \to +\infty$, f^κ degenerates into a Maxwellian VDF and $T_{\kappa\to\infty} = T_M$.

Beyond the fact that the Kappa VDF is convenient to model space plasma VDFs, there is an interesting property, pointed out by Scudder (1992a), which justifies its use. Indeed, if the VDF at the exobase is a Kappa function f_0^κ, the VDF at any distance r in the exosphere becomes then

$$f(v^2, r) = f_0^\kappa\left(\frac{v^2}{1 + \mathscr{V}^2(r)/\kappa v_{\kappa 0}^2}\right) \times \left(1 + \frac{\mathscr{V}^2(r)}{\kappa v_{\kappa 0}^2}\right)^{-(\kappa+1)} \quad (2.9)$$

where $\mathscr{V}(r)$ is defined by

$$\mathscr{V}^2(r) = 2\left(\phi_g(r) - \phi_g(r_0)\right) + \frac{2Ze}{m}\left(\phi_E(r) - \phi_E(r_0)\right), \quad (2.10)$$

It can be seen that this function keeps the shape of a Kappa VDF with the same index κ.

An ion-exosphere model with Kappa VDFs has been applied to the plasmasphere by Pierrard & Lemaire (1996). In the appendix, we describe the application of this new exospheric model to describe the coronal evaporation and solar wind flow.

2.4. Are the VDFs in the solar wind well represented by Kappa functions ?

Often the VDFs in space plasmas are observed to be quasi-Maxwellian up to the mean thermal velocities, while they have non-Maxwellian suprathermal tails at higher velocities or energies. The Kappa function is very convenient to model these VDFs, since it fits both the thermal as well as the suprathermal parts of the observed energy spectrae (Kivelson & Russell 1995). Up to now, the solar wind electron VDFs have usually been fitted to the sum of two isotropic Maxwellian VDFs: a core and a halo (see for instance Feldman et al. 1975). But as shown on Fig. 3 and previously pointed out by Vasyliunas (1968), a Kappa VDF is a more economic alternative to the core/halo model. In this Fig. we present a typical electron VDF in the solar wind, reported by Feldman et al. (1975) (see Fig. 16 in their paper). The diamonds represent the observed points of the VDF while the dashed lines represent the Feldman et al.'s double-Maxwellian core/halo fit. We have fitted the observed VDF with a Kappa model. The result is represented by the solid line in Fig. 3; the best fit for the suprathermal halo is obtained for $\kappa_e = 4.0$. Furthermore, we have shown that the variance of the dispersions between the observations and the model is slightly lower with the Kappa model (0.164) than with the core/halo one (0.172). Note, however, that the latter variances have been computed in the velocity range from ≈-2 10^7 m/s to ≈2 10^7 m/s and that, beyond 2 10^7 m/s, the Kappa model falls of more slowly than the observations. But at these higher energies and low flux values the reliability of the observations is also questionable.

The results obtained in this paper remain qualitatively valid when two Maxwellians (core/halo) VDFs are used to represent the velocity distribution of the electrons in the solar wind, instead of one single Kappa VDF. VDFs which have suprathermal tails can be considered to be produced by Scudder's (1992a) "velocity filtration" mechanism. Furthermore, Scudder (1992a) has shown graphically that the his mechanism can also lead to positive temperature gradients for any non-thermal distribution, in the same way he has demonstrated this analytically for the Kappa functions. Afterwards, Meyer-Vernet et al. (1995) have demonstrated analytically this property in the special case of a superposition of Maxwellians.

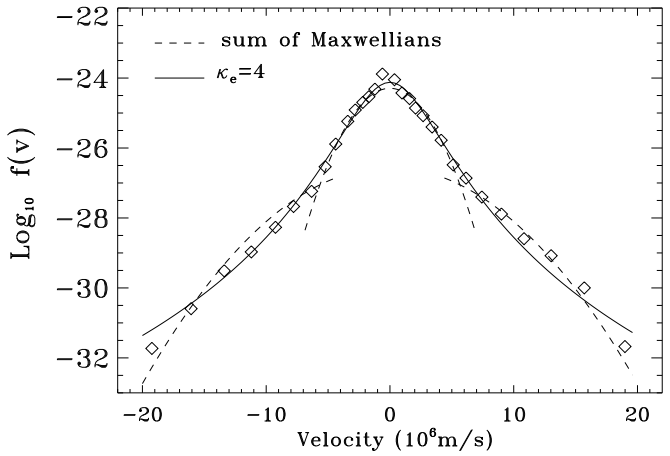

Fig. 3. Electron VDF in the solar wind (diamonds) as reported by Feldman et al. (1975). The dashed lines correspond to the classical model made of the sum of two Maxwellians: a core (n_c = 30.8 cm^{-3} and T_c = 1.6 10^5 K) and a halo (n_h = 2.2 cm^{-3} and T_h = 8.9 10^5 K). The full line represents our fit with a Kappa model (n = 33.9 cm^{-3}, T_κ = 1.9 10^5 K and κ_e = 4). Note that the Kappa model is is a more economic alternative since it needs one parameter less to fit.

2.4.1. The choice of the parameter κ

When a large number of solar wind electron VDFs, observed with the electron spectrometer on Ulysses, are fitted with Kappa functions, one find that the parameter κ_e globally ranges from 2 to 5 (Maksimovic et al., 1997).

Since the total potential energy for the protons is a decreasing function of the altitude, they all tend to escape and their evaporation flux does not significantly depend on the index κ_p of their VDF. This is one of the reasons why our model results presented in the next section are relatively insensitive to the value of κ_p. Thus, all the following results have been obtained for κ_p set equal to 500, i.e., the proton's VDF is assumed to be almost Maxwellian.

3. The results of the Kappa exospheric model

In this section, we present the plasma densities, bulk speed and temperatures obtained at 1 AU with our new exospheric model. In order to explore the influence of a change of the index κ_e, we have used four different values for the electron κ index: κ_e = 2, which is the lowest permissible value; κ_e = 3, κ_e = 6 and finally κ_e = 500, which coincides almost to a Maxwellian electron VDF.

3.1. The solar wind at 1 AU: model calculations

The electrical potential Φ_E (a), density n (b) and electron (c) and proton (d) average temperatures T_e and T_p obtained at 1 AU with our kinetic model are displayed in Figs. 4 a,b,c,d, as a function of the electron temperature T_{e0} at the exobase. The average temperatures are defined by $\langle T \rangle = (T_\parallel + 2T_\perp)/3$, $T_\parallel$ and $T_\perp$ derived from the pressure tensor components parallel and perpendicular to the magnetic field direction. As indicated in Table 1, the choice of a value for T_{e0} determines uniquely the other boundary conditions (T_{p0}, n_{p0}, n_{e0}) at the exobase. The five successive points on the curves shown in Fig. 4 correspond to the five sets of exobase condition given in Table 1. Each curve corresponds to a different value of κ_e.

3.2. Comparison with solar wind observations at 1 AU

The horizontal dotted lines in Fig. 4 correspond to the ranges within which the four physical quantities are usually observed at 1 AU. The density and proton temperature are usually observed to range between 1.0 and 30 cm^{-3} and between 10^4 and 2 10^5 K respectively (see Feldman et al. 1978). Taking into account the ranges within which the core/halo electron densities and temperatures were observed by Feldman et al. (1975), the average total electron temperature T_e range roughly between 5 10^4 and 1.2 10^6 K at 1 AU. The interplanetary electrical potential difference between the exobase and 1 AU can be determined assuming that the core/halo parametrization reflects the existence of two electron populations predicted by some previous exospheric theories of the solar wind (Jockers 1970; Schulz & Eviatar 1972; Perkins 1973). With this assumption, the core/halo breakpoint energy could be associated to the difference of electrical potential energy (Feldman et al. 1975; McComas et al. 1992). These authors found that the electrical potential at 1 AU, deduced from the breakpoint energy, ranges between 20 and 130 Volts.

It can be seen in Fig. 4 that the values of the density and temperatures observed at 1 AU and the electrical potential difference are well reproduced in our model with values of κ_e ranging between 2 and 6.

3.3. The high speed solar wind and its origins

The aim of this section is to compare the results on the solar wind expansion speed obtained with our kinetic approach to those of the classical hydrodynamic one.

3.3.1. The expansion speed at 1 AU

The expansion bulk speed at 1 AU obtained in our model is displayed in Fig. 5 as a function of T_{e0} and for three values of the κ_e index: κ_e = 2, κ_e = 3 and κ_e = 6. Note first a general tendency for the bulk speed V to increase with the temperatures at the exobase, T_{e0} and T_{p0}. Indeed, the average velocity of the escaping particles, which is the solar wind bulk speed, is an increasing function of the temperature and the width of the VDFs at the exobase: like in planetary atmospheres, when the width of a VDF is enhanced at the exobase, the number of particles with a velocity greater than the escaping velocity v_l is equally enhanced, and thus the average velocity of those particles is also increased.

But, as shown in Fig. 5, increasing the spread of the VDFs at the exobase is not the only way of increasing the solar wind bulk speed at 1 AU. The same result can be obtained for the electron VDF by decreasing κ_e. Indeed, we have shown that the

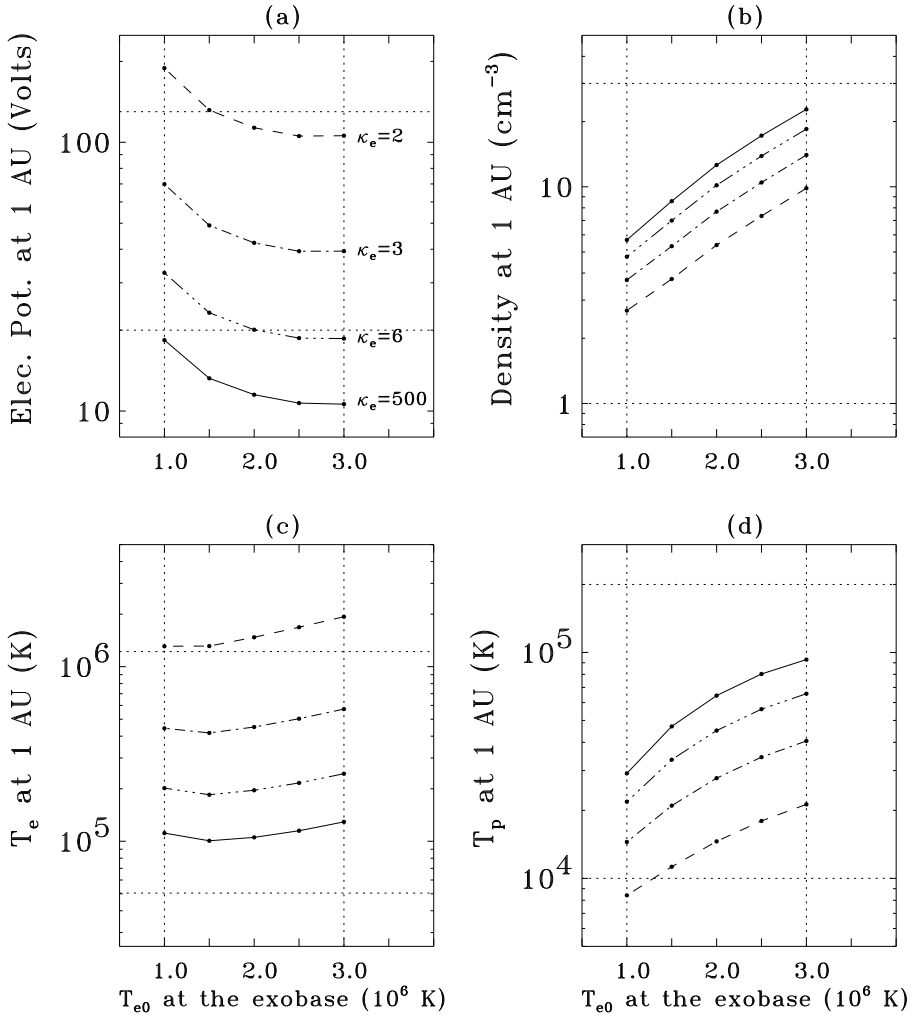

Fig. 4a–d. The electrical potential Φ_E (**a**), density n (**b**) and electron (**c**) and proton (**d**) average temperatures T_e and T_p obtained at 1 AU with the present kinetic model, as functions of the electron temperature T_{e0} at the exobase and for the four values κ_e = 2, κ_e = 3, κ_e = 6 and $\kappa_e = +\infty$.

average bulk velocity of the escaping particles increases when κ_e decreases; in other words:

$$\frac{\int_{v_l}^{+\infty} \mathrm{d}^3v\ v \cdot\ f^{\kappa}(v)}{\int_{v_l}^{+\infty} \mathrm{d}^3v f^{\kappa}(v)} \ \nearrow \text{ when } \kappa_e \ \searrow$$

This is the main result of the present study. It confirms a similar conclusion by Scudder (1992b), who analyzed the implication of his "velocity filtration " mechanism on the asymptotic form of Parker's (1963) isothermal solution for the bulk speed. Therefore, there is less need to refer to any additional (ad-hoc) heating mechanism in the outer corona, in order to increase the solar wind bulk speed, as it is often postulated in hydrodynamic model calculations.

In our model, the only physical input ingredients are the coronal density and temperatures at the exobase. Among the various hydrodynamic models of the solar wind, the one which is most comparable to our exospheric model, in terms of sophistication, is Parker's (1963) thermally driven solar wind model. This latter model does not include pressure anisotropies of the coronal fluid and no magnetic effects (which is equivalent to a radial magnetic field or a non rotating Sun); as our exospheric model, Parker's model is based on the assumption of a unique energy source: heat entering at the base of the corona which is converted into expansion bulk energy like in a de-Laval nozzle. Note also that Parker (1963) showed rather generally that the temperature achieved at the critical point determines the asymptotic wind speed in a way almost totally independant of the form of the energy equation. In Fig. 5 the solar wind bulk speed at 1 AU obtained from Parker's solutions (heavy dashed line) compare our exospheric approach. Parker's solutions have been computed for a spherical coronal expansion and a heliospheric temperature distribution of $T \propto r^{-0.5}$, which corresponds to an average gradient obtained from spacecraft observations. It is interesting to point out that Parker's bulk speed at 1 AU is almost identical to that for the kinetic solutions with Maxwellian VDFs or for $\kappa_e = \kappa_p = 500$. On the other hand, one can see in Fig. 5 that if one diminishes the value of κ_e below 6, then the Kappa exospheric model yields bulk speeds larger than the hydrodynamic one. Unlike the thermally driven hydrodynamic model, our exospheric model for the solar wind yields high bulk speed winds (600 - 800 km/s), provided the value of κ_e is small enough (2 - 3). Therefore our simple kinetic model of the solar wind leads to high velocities comparable to those obtained

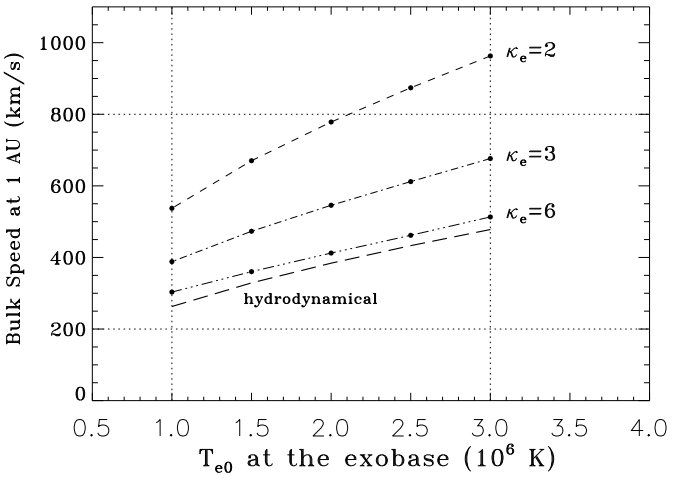

Fig. 5. The expansion bulk speed obtained at 1 AU with the present model, as a function of T_{e0} and for the three values κ_e = 2, κ_e = 3 and κ_e = 6: One can note that the high speed solar wind streams (600-800 km/s) can be explained if the electron VDFs in the corona have high velocity tails,,i.e., small values of κ_e (2-3).

in hydrodynamic models when additional MHD wave energy deposition is artificially added in the outer corona. Similar conclusions are reached by Scudder (1992b). Our work is therefore reinforcing his pioneering work.

3.3.2. The expansion speed/coronal temperature anticorrelation

In the second half of the 70's, the Skylab observations indicated that the coronal holes are the sources of the fast solar wind streams (Neupert & Pizzo 1974; Nolte et al. 1976; Krieger et al. 1973). The coronal holes plasma has a lower temperature than the equatorial active regions of the corona: $\approx 10^6$ K for the coronal holes and $\approx 2\ 10^6$ for the equatorial active regions (Withbroe & Noyes 1977). According to Parker's hydrodynamic model, the asymptotic solar wind bulk velocity decreases when the coronal temperature is lowered. The anticorrelation observed between the solar wind bulk speed and the coronal temperature seemingly has remained a puzzling feature for many years.

Our exospheric Kappa model offers an explanation for this anticorrelation. The three profiles of the bulk speed at 1 AU displayed in Fig. 5 have been obtained for constant values of κ_e. But, of course, the index κ_e may change with the temperature at the exobase. Indeed, as it is shown Table 1, the Coulomb collision times are very different for the case A ($\approx$ 1520 seconds) and for the case E ($\approx$ 160 seconds), assuming the radial electron density distribution remains the same in both cases. The difference is also important regarding the m.f.p. of the particles in the case A (3.4 $r_\odot$) and in the case E (0.7 $r_\odot$). Considering that non-Maxwellian features develop preferentially in cold and less dense coronal hole region, where the Coulomb collision time is large, one may infer that the value of κ_e for the low temperature model (A) can be smaller than that of the hotter models (B, C, D & E). Therefore, it is likely that in the case A the tail of the VDF at the exobase is more populated than in the case E: the value of κ_e for the case A should therefore be smaller than for the case E. Based on this hypothesis, Fig. 5 offers a possible explanation for the anticorrelation between the bulk speed observed at 1 AU and the coronal temperatures T_{e0} & T_{p0}. Indeed, from Fig. 5 and Table 2 it can be seen that in case A, corresponding to a low coronal temperature (T_{e0} = 10^6 K) but with a highly non-Maxwellian electron VDF (κ_e = 2), one obtains a higher speed solar wind at 1 AU, than for instance in the case C corresponding to a higher coronal temperature (T_{e0} = 2 10^6 K) and a nearly Maxwellian electron VDF (κ_e = 500). Fairfield & Scudder (1985) came to the same conclusion more than ten years ago. Our quantitative calculation reinforces their contention.

3.3.3. Conclusion

The results presented in this paper indicate that high speed solar wind streams can be explained provided the electron VDFs in coronal holes have enhanced high velocity tails, in contrast to the VDFs in the equatorial regions, which would be closer to that of a Maxwellian VDF due to the larger collision frequency there. It is possible also that the coronal magnetic field topology, whose effects have been neglected in the first series of exospheric models, plays a role by modifying the electron density and consequently the frequency of Coulomb collisions. In coronal holes the lines are "open", while in equatorial active regions there are closed loops where the particles can accumulate and collide more frequently. The consequence is that in the equatorial regions the Coulomb collision time is indeed smaller compared to that in the polar regions where magnetic field lines are more stretched out into interplanetary space. Therefore, the plasma should be closer to the Maxwellian equilibrium near the equator than in coronal holes. If the overall dipolar magnetic field topology of the Sun is the cause of the latitudinal density distribution, with higher densities at the equator than over the polar regions or in coronal holes, our assumption about the variation of the index κ_e versus heliographic latitude is then fully justified.

4. Summary

The present paper describes the first exospheric model (or zero-order kinetic model) of the solar wind based on Kappa velocity distribution functions for the electrons and protons escaping out of the corona.

1. We have shown that such kinetic models account rather satisfactorily for the main features of the solar wind. The electrostatic potential differences between the corona and the interplanetary space, the solar wind densities and temperatures obtained with these models fall within the ranges observed for these parameters at 1 AU.

2. In contrast with Parker's hydrodynamic models of the solar wind, with similar boundary conditions in the corona, the present kinetic model is able to predict the high speed solar wind without unreasonably large coronal temperatures and without

Table 2. The 1 AU bulk speed/coronal temperature anticorrelation

	Exobase	Parameters κ	Bulk Speed at 1 AU
Typical coronal hole conditions	A	κ_p = 500,κ_e = 2	547 km/s
Typical equatorial region conditions	C	κ_p = 500,κ_e = 500	333 km/s

additional heating of the outer region of the corona, as it is needed in hydrodynamic models to achieve the same solar wind speed.

3. Finally, our kinetic model offers a possible clue for a key feature of the solar wind flow which remained puzzling up to now, i.e., that the fastest solar wind flows originate from the coolest temperature regions in the corona (i.e., the coronal holes). It reinforces a similar conclusion obtained earlier by Fairfield & Scudder (1985): the electron VDFs in the cold coronal holes, which are the source of the high speed streams, posses an enhanced high velocity tail, which is simulated here by a Kappa function with a small value of κ_e, while in hot equatorial regions, from where the slow solar wind originates, the electron VDFs are closer to the Maxwellian equilibrium corresponding to $\kappa_e = \infty$.

Acknowledgements. We thank N. Meyer-Vernet for numerous comments and helpful suggestions on the manuscript.

Appendix A: the application of the generalized Lorentzian ion-exosphere model to the coronal evaporation and the solar wind flow

In this appendix we describe the application of the generalized Lorentzian ion-exosphere model, originally developed by Pierrard & Lemaire (1996), to the solar wind case. As indicated in the introduction, our new kinetic models are generalization of the ion-exosphere models by Lemaire & Scherer (1970; 1971a; 1973) which are based on Maxwellian VDFs.

A.1. The classes of particles

When the VDF is given at an exobase reference level, the VDF is then uniquely determined in the exosphere at higher altitudes in the collisionless region. The velocity space is divided into various domains corresponding to different classes of orbits in the gravitational potential $\Phi_g(r)$, electrostatic potential $\Phi_E(r)$ and magnetic field distribution which is assumed to have radial field lines corresponding to a non-rotating Sun. In order to characterize these different orbits, it is convenient to introduce $q(r)$, the dimensionless total potential energy of a particle by:

$$q(r) = \frac{m\Phi_g(r) + Ze\Phi_E(r) - m\Phi_g(r_0) - Ze\Phi_E(r_0)}{kT_0}$$

At r_0, $q = 0$. The radial distribution of q, for $r > r_0$, depends on the charge and mass of the particle. We consider a plasma containing electrons and protons only, i.e., without minor ionic constituants. In that case, it can be shown that the potential energy q_e for the electrons is a monotonically increasing function of the exospheric distance r, at least up to several AUs. This results from the fact that the electrical potential difference between the coronal exobase and infinity exceeds substantially the value Pannekoek-Rosseland potential (Lemaire & Scherer, 1969).

Thus, there are four possible classes for the electrons: trapped, incoming, escaping and ballistic electrons (see Tables I and II in Lemaire & Scherer, 1971a). In the present solar wind model, we consider only escaping, ballistic and trapped electrons: the incoming electrons are missing in the VDF. Since we assume that the trapped electrons are in thermal equilibrium with those which are escaping , the moments of the electron VDF up to the third order are given by the expressions (5) to (34) in Pierrard & Lemaire (1996).

For the protons, on the contrary, it can be shown that the potential energy q_p is a decreasing function of the exospheric distance r. As a consequence, there are no trapped nor ballistic protons: in our solar wind kinetic model all the protons are accelerated upwards and escaping out of the gravitational potential by the outward directed polarization electric field. In that case, the moments of the proton VDF are given by the expressions (40) to (44) and (50) to (52) in Pierrard & Lemaire (1996).

A.2. The electric potential

As already pointed out by Pikel'ner (1950), the use of the Pannekoek-Rosseland electric potential for the expanding corona is unrealistic because the escape flux of electrons exceeds the proton flux by a factor of $\sqrt{m_p/m_e}$, with the consequence that there would be a continuous positive charge deposition at the base of the corona. Thus a realistic electric potential $\Phi_E(r_0)$ at the exobase is that for which the flux of the accelerated protons is equal to the outward flux of escaping electrons. The flux of escaping electrons and the flux of protons are given respectively by Eq. (26) and Eq. (41) in Pierrard & Lemaire (1996). The value of $\phi_E(r_0)$ for which they are exactly equal, depends on the plasma density and temperatures at the exobase altitude r_0.The flux of protons is not very sensitive to the value of κ_p. On the contrary, the evaporation flux of the electrons is very

sensitive to the value of the index κ_e. This explains why the solar wind density, bulk speed and temperatures at 1 AU, predicted by our new exospheric model, are most dependent on the value of κ_e, but are relatively insensitive to the existence of a suprathermal tail in the proton VDF, i.e., to the value of κ_p.

Once the electric potential is determined at the exobase from the zero electric current condition, the radial distribution of $\Phi_E(r)$ is determined to satisfy the electrical quasi-neutrality equation at all the radial distances r: $\Phi_E(r)$ is obtained by solving the equation $n_p = n_e$, where the electron (n_e) and proton (n_p) densities are given by Eqs. (5), (25), (30) and (40) in Pierrard & Lemaire (1996). The solar wind exospheric density, particles fluxes and kinetic pressures can then be obtained by substituting $\Phi_E(r)$ in the expressions for the moments of the proton and electron VDFs.

References

Boltzmann L., 1875, Wien. Ber. 72, p. 427
Brandt J.C., Chamberlain J.W., 1960, Phys. Fluids 3, 485
Burlaga L.F., Ogilvie K.W., 1973, J. Geophys. Res. 78, 2028
Chamberlain J.W., 1960, ApJ 131, 47
Chen W.M., Lai C.S., Lin H.E., Lin W.C., 1972, J. Geophys. Res. 77, 1
Cuperman S., Harten A., 1970, ApJ 162, 315
Cuperman S., Harten A., 1971, ApJ 163, 383
Fairfield D.H., Scudder J.D., 1985, J. Geophys. Res. 90, 4055
Feldman W.C, Asbridge J.R., Bame S.J., Montgomery M.D., Gary S.P., 1975, J. Geophys. Res. 80, 4181
Feldman W.C, Asbridge J.R., Bame S.J., Gosling J.T., 1978 , J. Geophys. Res. 83, 2177
Griffel D.H., Davis L., 1969, Planet. Space Sci. 17, 1009
Hartle R.E., Barnes A., 1970, J. Geophys. Res. 75, 6915
Hartle R.E., Sturrock P.A., 1968, ApJ 151, 1155
Hollweg J.V., 1976, J. Geophys. Res. 81, 1649
Hundhausen A.J., 1972, Coronal expansion and Solar Wind, Spinger-Verlag, Berlin
Jeans J.H., 1923, The dynamical theory of gases, Cambridge Univ. Press, New York
Jockers K., 1970, A&A 6, 219
Kivelson M.G., Russel C.T., 1995, Introduction to Space Physics, Cambridge Univ. Press, p. 37
Krieger A.S.,Timothy A.F., Roelof E.C., 1973, Sol. Phys. 23, 123
Leer E., Holzer E., Fla T., 1982, Space Sci. Rev. 33, 161
Lemaire J., Scherer M., 1969, Compt. Rend. Acad. Sci. Paris 269B, 666
Lemaire J., Scherer M., 1970, Planet. Space Sci. 18, 103
Lemaire J., Scherer M., 1971a, Phys. Fluids 14, 1683
Lemaire J., Scherer M., 1971b, J. Geophys. Res. 76, 7479
Lemaire J., Scherer M., 1973, Rev. Geophys. & Space Phys. 11, 427
Lemaire J., Barakat A., Lesceux J.M., Shizgal B., 1991, in Rarefied Gas Dynamics, Ed. A.E. Beylich, VCH Verlags gesellschaft mbH, Aeronomica Acta A. 357, pp. 417
Maksimovic M., Pierrard V., Riley P., 1997, *Ulysses electron distributions fitted with Kappa functions*, submitted to Geophys. Res. Lett.
Maxwell J.C., 1873, Nat 8, 537,
McComas D.J., Bame S.J., Feldman W.C., Gosling J.T, Phillips J.L., 1992, Geophys. Res. Lett. 19, 1291
Meyer-Vernet N., Moncuquet M., Hoang S., 1995, Icarus 116, 202
Montgomery M.D., Bame S.J., Hundhausen A.J., 1968, J. Geophys. Res. 73, 4999
Neupert W.M., Pizzo V., 1974, J. Geophys. Res. 79, 3701
Newkirk G.J., 1967, ARA&A 5, 213
Nolte J.T., et al, 1976, Sol. Phys. 46, 303
Olbert S., 1982, in Solar Wind Five, ed. M. Neugebauer, NASA conference publication 2280, p. 149
Pannekoek A., 1922, Bull. Astron. Inst. Neth. 1, p. 107
Parker E.N., 1958, ApJ 128, 664
Parker E.N., 1963, Interplanetary dynamical processes, Interscience, New York
Perkins R.W., 1973, ApJ 179, 637
Pierrard V., Lemaire J., 1996, J. Geophys. Res. 101, 7923
Pikel'ner, S.B., 1950, Izv. Krymskoj Astrofiz. Obs. 5, 34
Pottasch S.R., 1960, ApJ. 131, 68
Rosseland S., 1924, MNRAS 84, 720
Schutz M.,Eviatar A., 1972, Cosmic Electrodynamics 2,402
Scudder J.D., 1992a, ApJ 398, 299
Scudder J.D., 1992b, ApJ, 398, 319
Shizgal B., 1977, Planet. Space Sci. 25, 203
Spitzer L. Jr., 1949, The Atmospheres of the Earth and Planets. In: Kuiper G.P. (ed.), Univ. Chicago Press III, p. 213
Spitzer L.Jr., 1962, Physics of fully ionized gases, Interscience, New York
Sturrock P.A., Hartle R.E., 1966, Phys. Rev. Lett. 16, 628
Vasyliunas V.M., 1968, J. Geophys. Res. 73, 2839
Whang Y.C., Liu C.K., Chang C.C., 1966, ApJ 145, 255
Withbroe G.L., Noyes R.W., 1977, ARA&A 15, 363
Withbroe G.L., 1988, ApJ 325, 442
Wolff C.L., Brandt J.C., Southwick R.G., 1971, ApJ 165, 181

This article was processed by the author using Springer-Verlag LaTeX A&A style file *L-AA* version 3.